

# EXTREMELY METAL-POOR STARS. VII. THE MOST METAL-POOR DWARF, CS 22876-032

John E. Norris

Research School of Astronomy & Astrophysics, The Australian National University,  
Private Bag, Weston Creek Post Office, ACT 2611, Australia; jen@mso.anu.edu.au

Timothy C. Beers

Department of Physics & Astronomy, Michigan State University, East Lansing, MI 48824;  
beers@pa.msu.edu

and

Sean G. Ryan

Physics Department, The Open University, Walton Hall, Milton Keynes MK7 6AA, United Kingdom; s.g.ryan@open.ac.uk

## ABSTRACT

We report high-resolution, high-signal-to-noise, observations of the extremely metal-poor double-lined spectroscopic binary CS 22876-032. The system has a long period :  $P = 424.7 \pm 0.6$  days. It comprises two main sequence stars having effective temperatures 6300 K and 5600 K, with a ratio of secondary to primary mass of  $0.89 \pm 0.04$ . The metallicity of the system is  $[\text{Fe}/\text{H}] = -3.71 \pm 0.11 \pm 0.12$  (random and systematic errors) – somewhat higher than previous estimates.

We find  $[\text{Mg}/\text{Fe}] = 0.50$ , typical of values of less extreme halo material.  $[\text{Si}/\text{Fe}]$ ,  $[\text{Ca}/\text{Fe}]$ , and  $[\text{Ti}/\text{Fe}]$ , however, all have significantly lower values,  $\sim 0.0\text{--}0.1$ , suggesting that the heavier elements might have been underproduced relative to Mg in the material from which this object formed. In the context of the hypothesis that the abundance patterns of extremely metal-poor stars are driven by individual enrichment events and the models of Woosley and Weaver (1995), the data for CS 22876-032 are consistent with its having been enriched by a zero-metallicity supernova of mass  $30 \text{ M}_\odot$ .

As the most metal-poor near-main-sequence-turnoff star currently known, the primary of the system has the potential to strongly constrain the primordial

lithium abundance. We find  $A(\text{Li}) (= \log (\text{N}(\text{Li})/\text{N}(\text{H})) + 12.00) = 2.03 \pm 0.07$ , which is consistent with the finding of Ryan et al. (1999) that for stars of extremely low metallicity  $A(\text{Li})$  is a function of  $[\text{Fe}/\text{H}]$ .

*Subject headings:* stars : nuclear reactions, nucleosynthesis, abundances – stars : abundances – stars : Population II – subdwarfs

*Suggested running title:* THE MOST METAL-POOR DWARF, CS 22876-032

## 1. INTRODUCTION

In the past two decades a handful of stars with heavy element abundance less than 1/1000 that of the sun ( $[\text{Fe}/\text{H}]^1 < -3.0$ ) have been analyzed at high spectral resolution, with a view to understanding the production of the elements at the earliest times. Such stars have the potential to constrain Big Bang Nucleosynthesis (Ryan, Norris & Beers 1999), the nature of the first supernovae (McWilliam et al. 1995; Ryan, Norris & Beers 1996; Nakamura et al. 1999), and the manner in which the ejecta from the first generations were incorporated into subsequent ones (Ryan et al. 1996; Shigeyama & Tsujimoto 1998; Tsujimoto & Shigeyama 1998; Ikuta & Arimoto 1999; Tsujimoto, Shigeyama & Yoshii 1999). In special cases, they can even be used to determine the age of the Galaxy (Cowan et al. 1999). As relatively simple objects, formed at redshifts  $\gtrsim 4$ –5, they nicely complement and constrain abundance results from the more complicated and less well-understood Lyman- $\alpha$  clouds and Damped Lyman- $\alpha$  systems currently studied at redshifts  $z < 3.5$  (see eg Ryan 2000).

The most metal-poor objects are generally faint, and studies to date have been undertaken with somewhat limited signal-to-noise (S/N). For the six stars having  $[\text{Fe}/\text{H}] < -3.5$  and so far analyzed at high resolution (see Table 6 of Ryan et al. 1996), perusal of the sources suggests that the data were obtained with a representative S/N per equivalent 0.04 Å pixel of roughly 30, corresponding to a  $3\sigma$  detection limit for weak lines of  $\sim 10$  mÅ. In some cases this has led to uncertainty as to the existence of important elements in these objects<sup>2</sup>. As one moves to the lowest abundances (or higher temperatures), the

---

<sup>1</sup> $[\text{Fe}/\text{H}] = \log (\text{N}_{\text{Fe}}/\text{N}_{\text{H}})_{\text{star}} - \log (\text{N}_{\text{Fe}}/\text{N}_{\text{H}})_{\odot}$

<sup>2</sup>For example, from Norris et al. (1996) : “Ba 4554 Å measurements of CD-38°245 are rather discordant, ranging from detection at 18 mÅ and 19 mÅ (Bessell & Norris 1984; Primas et al. 1994) to upper limits < 10 mÅ and < 7 mÅ by Molaro & Castelli (1990) and Peterson & Carney (1989).”

problem of determining reliable abundances can only deteriorate: for example, in the two near-main-sequence-turnoff dwarfs in the above-mentioned sample there are fewer than 20 non-Fe lines detected in the preferred wavelength range (3700–4700 Å), of which fewer than half are stronger than 20 mÅ.

To improve the accuracy of the existing abundance analyses we are attempting to obtain high resolution ( $R = 40,000$ ) data with  $S/N = 100$  of objects with  $[Fe/H] < -3.5$ . The purpose of the present work is to present results for CS 22876–032. In a subsequent paper we shall present results for CD–24°17504, CD–38°245, CS 22172–002, and CS 22885–096.

CS 22876–032 was discovered by Beers, Preston, & Shectman (1985), and with a high-resolution abundance determination of  $[Fe/H] = -4.3$  (Molaro & Castelli 1990; Norris, Peterson, & Beers 1993) it is currently the most metal-poor dwarf for which such analysis exists. The abundance determinations for this object are, however, compromised to some extent by the fact that it is a double-lined spectroscopic binary (Nissen 1989) of long but undetermined period. We set out to determine the nature of the two components and thus improve the reliability of the abundances in the system.

CS 22876–032 has the added attraction that it is the main-sequence dwarf closest in abundance to the material which emerged from the Big Bang. It therefore has a potentially important role in constraining the primordial abundance of Li, especially if the Li abundance in higher metallicity stars has been elevated by Galactic chemical evolution, as we contend elsewhere (Ryan et al. 1999). However, only after its atmospheric parameters have been reliably determined will one be in a position to fully realize that potential.

The outline of the paper is as follows. The observational material upon which our analysis is based is presented in § 2, while in § 3 we use the available material to present a first estimate of the period and orbital elements of the system. These results are coupled with the observed *BVRI* colors and available isochrones in § 4 to determine the atmospheric parameters  $T_{\text{eff}}$ ,  $\log g$ ,  $[Fe/H]$ , and  $\xi$  of the components, together with element ratios  $[X/Fe]$ . Finally, in § 5 we discuss the results and revisit the question of the Li abundance of the system, and its role in constraining the primordial value.

## 2. OBSERVATIONAL MATERIAL

### 2.1. High-resolution, High-signal-to-noise Spectroscopy

CS 22876–032 was observed with the University College London coudé échelle spectrograph, Anglo-Australian Telescope combination during sessions in August 1996,

1997, and 1998. The instrumental setup and data reduction techniques were as described by Norris, Ryan, & Beers (1996), and will not be discussed in detail here, except in particular instances where different techniques were dictated by the binarity of the system. Suffice it to say that the material covers the wavelength range 3700–4700 Å and was obtained with resolving power 40000. The numbers of detected photons in the spectra were 2700, 5800, and 3300 per 0.04 Å pixel at 4300 Å at the three epochs, respectively.

A comparison of the spectra in the region of the Ca II K line, registered to the rest frame of the primary of the system, is presented in Figure 1. Note the binary motion of the secondary as seen in the Fe I lines and the asymmetry of the Ca II line. In an effort to best use the effective  $S/N \sim 100$  of the combined data set, equivalent widths were determined for each binary component in two ways. First, since the lines of the two stars are well separated in the 1996 and 1997 data, the spectra from these epochs were co-added in the rest frame of each component in turn, and equivalent widths measured using techniques similar to those described in Norris et al. (1996). The second method utilized the relationship between central line depth and equivalent width. All three spectra were co-added in the rest frame of the relevant component, and central line depths measured. A quadratic was then fit to the dependence of these central depths on the equivalent widths which had been determined from the first method. This relationship was then used to determine equivalent widths for all lines having measured central depths. The final adopted equivalent widths,  $W_A$  and  $W_B$ , are the average of the two methods, and are presented in the final two columns of Table 1<sup>3</sup>. Throughout this work we shall denote the *observed* properties of primary and secondary with subscripts A and B, respectively, while for the inferred *intrinsic* parameters we shall use subscripts P and S. Based on the number of photons detected, we expect the equivalent widths to be accurate to 1–2 mÅ. The first three columns of the table present wavelength, excitation potential, and  $\log gf$  values from sources identified in Norris et al. (1996). For undetected species, limits of 5–10 mÅ are indicated in the table: these are a little larger than  $\sim 3\sigma$  limits based on photon statistics, and are commensurate with the detectability of lines on the spectra. A comparison of the present results for CS 22876–032 with those of Molaro & Castelli (1990) and Norris et al. (1993) is presented in Figure 2, where one sees that the presently derived equivalent widths are somewhat smaller than reported by them. We conjecture that this may have resulted from the continuum having been placed too high on the lower  $S/N$  spectra in these earlier investigations.

For lines stronger than 10 mÅ in both members of the system, Figure 3 compares the

---

<sup>3</sup>It may be of interest to some readers to compare our final equivalent widths with those determined with the first, more standard, method. The mean difference between final and first estimates is less than 1% for both primary and secondary. The mean absolute differences are 4 and 6 %, respectively.

ratio of primary to secondary equivalent widths as a function of primary line strength, wavelength, and excitation potential. One sees little, if any, dependence on wavelength and excitation, but an apparent correlation with line strength. Note too the much smaller scatter in the  $W_A/W_B$  vs  $W_A$  diagram, which is more commensurate with our error estimates, shown in the figure for  $\sigma_W = 2$  mÅ. This may be understood in terms of curve-of-growth effects, to which we shall return in § 4.1.

In § 5.2 we shall introduce spectra taken at longer wavelengths to determine the strength of the Li I 6707 Å line. These data permitted us to determine the strength of the Mg I b lines in both components, which are also presented in Table 1. The S/N per 0.04 Å bin at  $\lambda 5180$  Å was 55.

## 2.2. Radial Velocity Data

Table 2 contains the radial velocities for CS 22786–032 which we have been able to glean from the archives of the Anglo-Australian Observatory (principally from our own observations), literature material kindly provided by Drs. P.E. Nissen and J.A. Thorburn, and a service observation from the William Herschel Telescope. For the AAO and WHT data we measured velocities using techniques similar to those described by Norris et al. (1996), which we shall not repeat here and to which we refer the reader. The information in the table should be self-explanatory, except perhaps for the errors, which provide an estimate of combined internal and external uncertainties.

## 2.3. *BVRI* and Strömgren Photometry, and Interstellar Reddening

Broad-band *BVRI* photometry is available for CS 22876–032 from the work of Norris et al. (1993), following whom we adopt  $B-V = 0.395$ ,  $V-R = 0.28$ , and  $R-I = 0.31$ . These values have uncertainties of 0.01 mag. Strömgren photometry is available from Schuster, Parrao, & Contreras Martinez (1993) and Schuster et al. (1996):  $b-y = 0.334$ ,  $m_1 = 0.036$ , and  $c_1 = 0.245$ , with uncertainties  $\sim 0.005$ . Following the latter authors we adopt  $E(B-V) = 0.00$ , based on the analysis of their Strömgren data. Beers, Preston, & Shectman (1992) report  $E(B-V) = 0.01$  for CS 22876–032 in good agreement with this value, suggesting that the reddening is well-determined, with uncertainty 0.01 mag.

### 3. ORBITAL ELEMENTS

The 21 radial velocity measurements are sufficient to constrain considerably the orbital elements of this system. In Figure 4a we present the periodogram of the primary, determined using the procedure of Lafler & Kinman (1965). Our best estimate of the period from this method is  $\sim 425$  days. Values corresponding to other less prominent dips in the figure result in the phased velocity diagram having considerably larger scatter than is seen for this value.

An initial estimate of the orbital elements for the two components was obtained by first setting the orbital period fixed at 425 days, and solving only for the elements of the primary using the method of Russell-Wilsing (Russell 1902; re-discussed by Binnendijk 1960). We then obtained estimates of the orbital elements for both the primary and secondary of CS 22876–032 following the differential corrections procedure of Lehmann-Filhés (1894; re-discussed by Underhill 1966), using code kindly made available to us by Dr. R.D. Mathieu (private communication). The code we employed, SBOP, is an adaptation of a FORTRAN II code originally listed by Wolfe, Horak, & Storer (1967). Solutions were attempted with an application of equal weights to all observations, followed by a de-weighting of the two observations made with the RGO spectrograph, in order to reflect their lower velocity accuracy. The elements which were obtained were quite similar in both cases. Results are presented in columns (2) and (3) of Table 3. The observational data, phased to these elements, together with the model radial velocity curves for primary and secondary are presented in Figure 4b. The agreement is quite satisfactory.

At the suggestion of the referee, we have attempted to obtain orbital solutions with starting values for the period centered around the less prominent dips in the periodogram, at  $P \sim 316$  and  $P \sim 500$  days, respectively. In both instances, SBOP failed to converge to a satisfactory solution, consistent with our expectations. As a check on the sensitivity to the initial guess of the orbital period, we have also sought solutions with starting values for the period in the range 405 to 450 days. Outside this range of initial periods, SBOP again failed to converge to a solution. For starting points within the above range, SBOP converged to the same final period estimate, and the same set of orbital parameters as when we chose a starting period of 425 days. We conclude that our final solutions are stable, and accurate to the limit which the present data allow. Future spectroscopic study of CS 22876–032 will allow us to more fully populate the phase diagram, and hence enable refinement of the derived orbital elements.

The errors on all of the estimated elements are also listed in Table 3. As can be seen from inspection of the table, the elements are well constrained with the exception of the time of periastron passage ( $T_0$ ) and the angle of periastron passage ( $\omega$ ). This is perhaps to be

expected given the low eccentricity of this system ( $e \sim 0.12$ ) and the relatively sparse phase coverage of our measurements. The mass ratio of the system  $M_S/M_P = 0.89 \pm 0.04$  provides a useful confirmation of our attempt at deriving appropriate atmospheric parameters for the two components by comparison with model isochrones, discussed below. Even though the error in  $T_0$  is larger than we would like, it corresponds to only 0.03 in phase, so one still obtains useful predictions of optimal observing opportunities when the components are expected to show the greatest velocity separation.

For heuristic purposes we present in column (4) of the table the changes to the elements which were obtained when the two most discrepant data points (which have large observational uncertainties) were removed from the data set. While this leads to elements with slightly improved errors, it is interesting to note that the differences are well within the cited errors in column (3).

We now consider whether CS 22876–032 is an eclipsing system. Given the large separation of this pair of dwarfs the likelihood is not great. Assuming solar diameters, we estimate that the chance of eclipse is less than 0.02, and its duration less than one day. We also note that while the period of the system is established to  $\sim 0.6$  day, the zero point of the ephemeris is known to only 14 days, which will make the search for eclipse more difficult. That said, the additional insight to be obtained from eclipse information would seem to warrant such an effort.

## 4. ATMOSPHERIC PARAMETERS

### 4.1. $T_{\text{eff}}$ , $\log g$ , [Fe/H]

One may use the observed  $BVRI$  and Strömgren colors together with stellar evolutionary isochrones to constrain the atmospheric parameters of the components of the system.

With  $(B-V)_0 = 0.395$ , CS 22876–032 could in principle comprise a system having either two objects below the halo main-sequence turnoff, or a system with one or both objects above it. The Strömgren  $c_1$  value of 0.245, however, which is typical of metal-poor main sequence dwarfs (see Schuster et al. 1996), clearly requires that both objects lie below the turnoff. If, for example, one forms composite colors from pairs of models on the VandenBerg & Bell (1985) isochrones with  $Y = 0.20$ ,  $Z = 0.0001$ , and age = 14 Gyr, one finds that with  $B-V \sim 0.40$ ,  $c_1 \sim 0.35$  for those containing at least one star above the turnoff, and  $c_1 \sim 0.25$  for those with both below it. In what follows, therefore, we shall assume that both components of CS 22876–032 lie below the main sequence turnoff.

For convenience we illustrate our method using the Revised Yale Isochrones (Green, Demarque, & King 1987 (RYI)), for  $Y = 0.20$ ,  $Z = 0.00001$  ( $[\text{Fe}/\text{H}] \sim -2.3$ ), and age = 13 Gyr, and later comment on its sensitivity to these choices. Figure 5a,b show the locus of isochrone pairs of  $B-V$  and of  $T_{\text{eff}}$  values which together combine to produce the value  $(B-V)_0 = 0.395$  observed for CS 22876–032. One sees that only a narrow range of permitted color and  $T_{\text{eff}}$  exists for the primary, and one can thus constrain the parameters for this component quite well. The situation is not so favorable for the secondary, but once the primary is specified one can constrain the secondary by requiring that both stars have the same metallicity. An iterative procedure, which converged quickly, is described below.

For any isochrone pair one may also determine the equivalent width correction factors one should apply to observed line strengths to obtain intrinsic values. (The corrected equivalent widths are obtained by multiplying the observed ones by these factors.) The correction factors  $f_1$  and  $f_2$  are the reciprocals of the fractional flux contributions of the two components, so  $1/f_1 + 1/f_2 = 1.0$ , and the primary:secondary luminosity ratio is simply  $f_2/f_1$ . The values are inferred directly from the isochrones. Strictly, the  $(f_1, f_2)$  values are wavelength dependent, but in practice a single pair suffices throughout the blue-violet spectral region. We note for completeness that the values adopted here are determined at the effective wavelength of the B band. Fluxes are sufficiently different in the red spectral region, however, that red-specific ratios must be utilized for the analysis of Li 6707 Å (see below). In Figure 5c we show the locus of pairs of correction factors applicable in the blue-violet region.

Similar diagrams may be constructed for  $V-R$  and  $R-I$ . Given the observational data of Table 1, one is now in a position to determine abundances for model pairs which reproduce the observed colors. We refer the reader to Ryan, Norris, & Beers (1996) for the details of our model atmosphere abundance determination technique, which are quite standard and which we shall not repeat here, except to note that we employ Bell (1983) models in our analysis. Figure 6 shows the dependence of  $[\text{Fe}/\text{H}]$  on  $T_{\text{eff}}$  for several pairs of permitted primary, secondary pairs, determined when using atmospheric parameters based on  $B-V$ . By adopting the requirement that both components have the same value of  $[\text{Fe}/\text{H}]$  (to within 0.01 dex) we then remove the degeneracy of the procedure. Similar diagrams were constructed using  $V-R$  and  $R-I$  rather than  $B-V$  to constrain the atmospheric parameters. Table 4 contains the results, where column (1) presents the observed composite color, columns (2), (3), (4), and (5) contain the mass,  $T_{\text{eff}}$ , color, and equivalent width correction factor for the primary, respectively, and columns (6)–(9) give the same parameters for the secondary. Assigning equal weight to the values for each of the three cases we find that the system has  $[\text{Fe}/\text{H}] = -3.71$  and that the masses are  $0.83$  and  $0.73 M_{\odot}$ . The average mass ratio is 0.88, in pleasing accord with the analysis of orbital parameters in § 3. Finally, in

Table 5 we present our adopted atmospheric parameters for the components of the system.

In Figure 3 we showed that the ratio of observed equivalent widths,  $W_A/W_B$ , increases with line strength. The equivalent width correction factors derived in the decomposition of the binary,  $f_{4300,P}$  and  $f_{4300,S}$ , are listed in Table 4 and aid in explaining the observed variation of the ratio of the observed equivalent widths. Specifically, the large value of  $f_{4300,S}$  indicates that the *apparently* weak lines in the secondary ( $W_B$  in the range 8–24 mÅ) are in reality stronger by a factor  $\sim 4.6$  in the uncontaminated spectrum, and thus occupy the moderately strong range  $37 \leq W_S \leq 110$  mÅ, partially on the flat part of the curve of growth. The primary, on the other hand, has only a factor 1.28 difference between its observed ( $W_A$ ) and intrinsic ( $W_P$ ) values, confirming that most of its lines do indeed lie on the linear portion of the curve of growth. The increase in the ratio  $W_A/W_B$  is therefore understood as the progressive saturation of the secondary’s lines with increasing line strength, while those of the primary are not so affected.

We illustrate this in Figure 7, which compares the observations with theoretical line ratios computed for two stars having the adopted parameter set. The theoretical curve reproduces the observed behavior quite well, confirming the origin of this effect. The reader might comment that the agreement is less than satisfactory for  $W_A > 40$  mÅ, and we would have to concur. We note, however, that it is in this regime that the lines of the secondary have  $W_S \sim 100$ –140 mÅ and experience strong saturation effects. It is not unlikely that uncertainties in the relatively poorly-defined adopted microturbulence of the secondary and the treatment of van der Waals broadening (see e.g. Ryan 1998) might lead to significant error in the theoretical strengths of these lines.

## 4.2. Error Budget

How robust are the abundances and atmospheric parameters in Tables 4 and 5? The answer is somewhat complicated because of the interplay of the two components of the binary. We discuss random and systematic errors, including the impact of one star upon the other, and summarize the situation in Table 6.

First consider the uncertainties in the adopted atmospheric parameters. Errors in color-effective temperature transformations of  $\sim 100$  K are (unfortunately) common in the analyses of metal-poor stars. If the two components of the system were of comparable spectral type, both would be affected similarly by this error source. Since, however, their temperatures differ by 700 K, independent errors of 100 K are allocated to each. Additionally, errors in photometry and reddening are 0.01 mag, each yielding an additional

uncertainty of 40–60 K. The adopted error in each star’s  $T_{\text{eff}}$ , summing in quadrature, is therefore 130 K. We note that this is consistent with the range of temperatures derived in Table 4 for the three photometric colors. The error in  $T_{\text{eff}}$  for the secondary, however, has almost no impact on the derived  $[\text{Fe}/\text{H}]$  of the system, as can be seen in Figure 6, since an incorrect temperature will be compensated for by a change in the derived  $f_{\text{s}}$  factor. We assign 0.10 dex and 0.03 dex as the error in  $[\text{Fe}/\text{H}]$  induced by the primary and secondary stars’ temperature uncertainties, respectively. We adopt the sensitivity to errors in microturbulence and surface gravity from the calculations, but apply only those due to the primary, again because of the weak sensitivity to the secondary’s parameters.

Taking all atmospheric parameter uncertainties into account the quadratic sum of errors in  $[\text{Fe}/\text{H}]$  is 0.11 dex.

Errors in the parameters of the primary and secondary also change the inferred mass ratio of the system. There is little latitude for the mass of the primary, as indicated by the small range of  $T_{\text{eff}}$  and  $f_{\text{p}}$  values in Figure 6. However, the temperature and mass inferred for the secondary will vary if the primary is revised. Changes in the primary corresponding to  $\Delta[\text{Fe}/\text{H}] = 0.11$  dex (from above) would induce a change in the secondary corresponding to 0.02 in the mass ratio. The small sensitivity of the mass ratio to the decomposition of the system is confirmed in Table 4, where the range of values is 0.015.

Additional errors are associated with the adoption of a particular model atmosphere grid, which can lead to differences of 0.10 dex (Ryan et al. 1996, § 3.2), and in the isochrones used in the decomposition of the binary. The latter effect was assessed by changing the adopted RYI isochrone and viewing the impact on the derived parameters of the binary. Reasonable changes in helium, heavy element abundance, and age, of  $\Delta Y = 0.05$ ,  $\Delta \log Z = 0.5$ , and  $\Delta \text{Age} = 2$  Gyr, respectively, lead to changes in the abundance of the primary  $\Delta[\text{Fe}/\text{H}] < 0.04$ . The corresponding change in the mass ratio is also small,  $\simeq 0.02$ .

We also repeated the temperature and abundance determination exercise at  $Z = 0.0001$  for the isochrones of the RYI, of Bergbusch & VandenBerg (1992) and those of the Padua group available in 1999 October at <http://dns2.pd.astro.it/>. Using  $B-V$  to constrain the temperature we obtained  $[\text{Fe}/\text{H}]_{\text{P}} = -3.52$ ,  $-3.51$ , and  $-3.38$ , respectively. The difference between the value obtained by adoption of the Padua and the others is driven essentially by a difference in their adopted  $B-V$ ,  $T_{\text{eff}}$  transformation, the role of which has already been considered above. We conclude, therefore, that our abundance determination for CS 22876–032 is insensitive to the adoption of the Revised Yale Isochrones.

The summary of the error budget is shown in Table 6, where column (1) lists the error source, column (2) the representative error in the parameter, and column (3) the error in

the abundance of the primary (and hence of the system) or  $M_S/M_P$ , as appropriate. Given these errors we conclude that the abundance of CS 22876–032 is  $-3.71 \pm 0.11 \pm 0.12$ , where the first and second uncertainties refer to random and systematic errors, respectively.

It is of interest to compare this value with the significantly lower abundances reported by Molaro & Castelli (1990) and Norris et al. (1993), who found  $[\text{Fe}/\text{H}] = -4.29$  and  $-4.31$ , respectively. For illustrative purposes we show in Table 7 abundance changes which result from various sources between the present value and that of Norris et al. (1993). In all but two cases the parameters and assumptions made in the present work lead to a higher abundance, accumulating to  $\sim +0.4$  when taken one at a time — not too much below the reported difference of  $+0.6$ . Although CS 22876–032 is still the most metal-poor dwarf known, our current best estimate of its metallicity is considerably less extreme than the first measurements.

We complete the discussion by noting that in our high-resolution studies and those of McWilliam et al. (1995) no halo dwarf *or* giant is known with  $[\text{Fe}/\text{H}] < -4.0$ . The low-resolution surveys of Beers and his co-workers also strongly suggest that the metallicity distribution of the Galactic halo cuts off near this value (e.g. Beers et al. 1998; Norris 1999).

### 4.3. Relative Abundances, $[\text{X}/\text{Fe}]$

Using the techniques described in some detail in Ryan et al. (1996) we next computed the abundances of the other elements. Results for the two components are presented in Table 8, where the column headers should be self-evident except perhaps for column (2), which gives details of the features used in the abundance determination. At the metal weakness of CS 22876–032, one has in most cases only one or two lines from which to determine the abundance. If only one feature is available we give its wavelength in column (2); otherwise the number of lines involved is tabulated. The standard errors given in columns (5) and (7) were determined using techniques described by Ryan et al. (1996, § 4.3). In brief, they represent the quadratic addition of abundance errors due to uncertainties in the atmospheric parameters and the measurement of line strengths. The reader should note that our knowledge of the abundances of elements, other than Fe, observed in CS 22876–032 is based on only eight atomic lines.

Table 8 also contains abundance limits for a number of elements which are more stringent than previously available, given the higher S/N of the present investigation. We note that in most cases limits are given only for the primary of the system, since they are

not very useful for the secondary.

The present data permit us to revisit the Mn abundance of CS 22876-032. The contrast between the previous Mn I 4030 Å measurement of  $W = 20$  mÅ (Molaro & Castelli 1990; S/N  $\simeq 55$ –100 at  $R \simeq 20000$ ), and ours at  $W_A < 5$  mÅ (S/N  $\simeq 100$  at  $R \simeq 40000$ ) highlights yet again (if such a comment is necessary) the need for high S/N and resolving power to study weak lines. In the absence of a definitive test, we note that the new measurement leads to a Mn abundance which more closely resembles that of other stars at this [Fe/H].

With one exception the abundances determined for the two components of CS 22876–032 are in excellent agreement, consistent with the atmospheric parameters of both objects having been well determined. The exception is Si for which the relative abundances disagree by 0.50, a difference formally significant at the  $1.9\sigma$  level. In comparison, the mean absolute difference for the four other elements observed in both components is 0.05 dex. Although a  $1.9\sigma$  difference is not highly significant, we have scrutinized all of our spectra of this line. We find no reason beyond the formal errors for mistrusting this measurement. However, we remain also at a loss to explain the different Si abundances in the two components.

## 5. DISCUSSION

### 5.1. Heavy Element Abundances

Evidence has mounted over the past decade that below  $[\text{Fe}/\text{H}] = -3.0$ , Galactic chemical enrichment was a rather patchy business (e.g. Ryan, Norris & Bessell 1991; McWilliam et al. 1995; Ryan et al. 1996), leading to models in which such metal-poor objects are formed in the interaction of supernova remnants with material in their immediate vicinity (Ryan et al. 1996; Tsujimoto et al. 1999). In such models, one expects the abundance patterns of the most metal-poor stars to be representative of individual supernova, rather than of a time-averaged ensemble. Hence, high-resolution spectroscopic analyses of extremely metal-poor stars provide a powerful probe of the nature of the first supernovae in the Milky Way.

Given the paucity of lines in CS 22876–032 we have only Al and the  $\alpha$ -elements to discuss. In the context of star-to-star scatter we shall defer further consideration until we present results on the other four extremely metal-poor stars for which we have data, and which we mentioned in § 1 – except to note here that the value  $[\text{Al}/\text{Fe}] = -0.44$  for CS 22876–032 lies within  $\sim 0.20$  of the mean line determined for the sample of metal-poor stars discussed in the investigation of Ryan et al. (1996, Figure 3).

In the spirit of associating the yields of particular supernovae models with the observed abundances in extremely metal-poor stars, we conclude by discussing the  $\alpha$ -elements. For Mg, which is produced mainly during hydrostatic carbon and neon burning we find  $[\text{Mg}/\text{Fe}] = 0.50$ . For Si and Ca we find a weighted mean value, which we designate  $[\langle \text{Si}, \text{Ca} \rangle / \text{Fe}]$ , of  $-0.05$  (the data were weighted by the inverse square of their errors). These elements are produced by a combination of hydrostatic oxygen shell burning and explosive oxygen burning, which varies from star to star (Weaver & Woosley 1993). As discussed by Woosley & Weaver (1995), the predicted yields of Si and Ca are expected to vary relative to Mg, depending sensitively on several physical effects. (These include among others the treatment of convection, the density structure near the iron core, the location of the mass cut, and the amount of material which falls back in the explosion.) For CS 22876–032 we have  $[\langle \text{Si}, \text{Ca} \rangle / \text{Mg}] = -0.55$ . It is then interesting to consider the production factors of the zero-heavy-element model supernovae of Woosley & Weaver (1995, Table 17). For those models which produce significant amounts of Mg, Si, and Ca we find the results presented in Figure 8. If one were to seek to interpret the data for CS 22876–032 in terms of enrichment from a single zero-heavy-element supernova one could identify it, quite reasonably, with the Woosley & Weaver (1995)  $30 \text{ M}_\odot$  model Z30B.

Titanium is produced under more extreme conditions than Si and Ca, as discussed by Woosley & Weaver (1995). In CS 22876–032, as for Si and Ca,  $[\text{Ti}/\text{Fe}]$  is low relative to  $[\text{Mg}/\text{Fe}]$ : we find  $[\text{Ti}/\text{Mg}] = -0.39$ . This is also best reproduced by Woosley & Weaver model Z30B.

Is our result of  $[\text{Al}/\text{Mg}] = -0.94 \pm 0.17$  consistent with the hypothesis? Before comparison with theory one must correct the present LTE abundance for Al for non-LTE effects. According to Baumüller & Gehren (1997), LTE abundances for Al based on the line we have used underestimate the abundance by  $\sim 0.65$  dex at  $[\text{Fe}/\text{H}] \sim -2.5\text{--}3.0$ . Adopting this correction for CS 22876–032, one therefore has  $[\text{Al}/\text{Mg}] \sim -0.3 \pm 0.2$ . For the above-mentioned models of Woosley & Weaver (1995), in comparison, one finds  $[\text{Al}/\text{Mg}]$  in the range  $\sim -0.65\text{--}-0.35$ . That is, the models do not strongly constrain the situation, and within the observational errors one has reasonable agreement between theory and observation.

## 5.2. Lithium Abundance

Given the improved atmospheric parameters for the components of CS 22876–032, one may revisit the question of its lithium abundance. The best currently available observational material is that of Thorburn & Beers (1993). They obtained data with  $\text{S/N} = 150$  and

reported  $W_A(\text{Li I } 6707\text{\AA}) = 11 \pm 1.3 \text{ m\AA}$  at JD 2448850.8, when the lines of the two components were well separated. They did not detect the Li line in the secondary. Norris et al. (1994) have also observed this object and report  $W_A(\text{Li I } 6707\text{\AA}) = 15 \pm 2.1 \text{ m\AA}$  from a spectrum with  $S/N = 70$ , obtained at JD 2448490.5 when the lines of the primary and secondary would have been well separated, by some  $20 \text{ km s}^{-1}$ .

As part of our continuing interest in the lithium problem we attempted to remeasure the equivalent width during an observing run on the Anglo-Australian Telescope in 1999 September, using techniques similar to those described by Norris et al. (1994) and Ryan, Norris, & Beers (1999). From a spectrum having  $S/N = 70$  per  $0.04 \text{ \AA}$  increment we obtain  $W_A(\text{Li I } 6707\text{\AA}) = 14.4 \pm 2.3 \text{ m\AA}$ . At the time of observation the lines of the primary and secondary were separated by  $21 \text{ km s}^{-1}$ , and the line in the secondary was below our threshold of detectability, which we estimate to be  $7 \text{ m\AA}$  ( $3\sigma$ ).

We seek to compare these data with the recent accurate and homogeneous observational material of Ryan et al. (1999). We first ask if there are systematic equivalent width errors between the various authors. For 16 stars in common between Ryan et al. (1999) and Thorburn (1994) (who used the same equipment and techniques as those of Thorburn & Beers) one finds  $\langle W_{\text{RNB}} - W_{\text{T}} \rangle = -1.9 \pm 1.1 \text{ (s.e.) m\AA}$ , while for 5 stars in common between Ryan et al. and Norris et al. (1994) one finds  $\langle W_{\text{RNB}} - W_{\text{NRS}} \rangle = +2.3 \pm 1.7 \text{ (s.e.) m\AA}$ . We do not regard these differences as statistically significant, and make no correction to the reported equivalent widths. We then adopt  $W_A(\text{Li I } 6707\text{\AA}) = 12.5 \pm 1.4 \text{ m\AA}$  as the best currently available value for CS 22876-032, having weighted the data by the inverse square of their estimated errors. (The error is based on small sample statistics following Keeping (1962) without cognisance of the weights.) At  $\lambda 6707\text{\AA}$  our model shows that to obtain the line strength intrinsic to the primary this should be corrected by the factor  $f_{6707,\text{P}} = 1.35^4$ , which leads to  $W_{\text{P}}(\text{Li I } 6707\text{\AA}) = 16.9 \pm 1.9 \text{ m\AA}$ .

The recent study of Li by Ryan et al. (1999) used an effective temperature scale different from the RYI one that accompanies the isochrones used in the decomposition of the binary. It would be inappropriate to compare the Li abundance of CS 22876-032 computed using the RYI temperature scale, with a set of data based on an entirely different one. For this reason, we use the decomposed *colors* of the binary, as given in Table 4, to infer the temperature on the same scale as our 1999 Li work. We obtain  $T_{\text{eff}} = 6223 \pm 38 \text{ K}$ .

---

<sup>4</sup>Based on *B-R* results from the RYI and on model atmosphere synthetic spectra, which give consistent results.

The inferred lithium abundance<sup>5</sup>  $A_P(Li)$  ( $= \log (N_P(Li)/N_P(H)) + 12.00$ )  $= 2.03 \pm 0.07$ <sup>6</sup>. (The uncertainty in the quadratic addition of errors corresponding to  $\Delta f_{6707,P} = 0.01$ ,  $\Delta T_{eff} = 38$  K, and  $\Delta W_P(Li I 6707\text{\AA}) = 1.9$  m\AA. We recall that here ‘P’ by convention refers to ‘Primary’ and not necessarily ‘Primordial’.)

The non-detection of the secondary by Thorburn & Beers (1993) and the present work is also important. If this component has  $T_{eff} = 5600$  K and the same Li abundance as the primary, one would expect an intrinsic line strength  $W_S(Li I 6707\text{\AA}) = 45$  m\AA. Applying a model correction factor  $f_{6707,S} = 3.9$  (applicable at  $\lambda 6707$  \AA for the secondary), the observed line strength would then be 12 m\AA. The most likely explanation for the non-detection of Li in the secondary is that with  $T_{eff} = 5600$  K it lies at the cool edge of the Spite Plateau and has experienced modest depletion to below its primordial value. The uncertainty in the temperature of the secondary is also greater than that of the primary, as is evident from Figure 6, and could explain part of the problem.

From their investigation of an unbiased sample of 23 near-main-sequence-turnoff stars having  $6050 < T_{eff} < 6350$  K and  $-3.6 < [Fe/H] < -2.3$  Ryan et al. (1999) reported a dependence of  $A(Li)$  on  $[Fe/H]$ . Their “best fit” was  $A(Li) = 2.447(\pm 0.066) + 0.118(\pm 0.023) \times [Fe/H]$ . They argued that the most likely explanation of the positive trend with metallicity was that the primordial lithium abundance had been increased by early Galactic chemical enrichment involving the interaction of cosmic rays with the interstellar medium (see also Ryan et al. (2000)). Their material and its “best fit” trend, together with the present result for CS 22876–032, are presented in Figure 9. It is clear that the data for the latter object, which is currently the lowest metallicity dwarf known, are completely consistent with the trend reported by Ryan et al. and support their hypothesis. Equally

---

<sup>5</sup>The Li abundance was calculated using exactly the same formalism as in Ryan et al. (1999), i.e. computing synthetic spectra for Bell (1983) models using four  $^7Li$  components, and measuring the equivalent width of the synthesized line.

<sup>6</sup>The perceptive reader will note that in this work we have combined the higher S/N data of Thorburn & Beers (1993; S/N = 150) with our lower S/N data (two spectra each with S/N = 70), whereas in a recent work (Ryan et al. 1999) on the spread about the plateau we advocated the importance of homogeneity. We would not advocate the coaddition of data were we studying the spread here, since the statistic used to describe spread – the standard deviation – is acutely sensitive to errors, which enter as squared terms. However, the current comparison is with the mean abundance of the stars, and the mean is less affected than the standard deviation by divergent phenomena. Consequently we have chosen to use the superior-S/N data of Thorburn & Beers as well. We note that if we instead adopted only the less accurate (S/N-limited) value of  $W_A = 14.4 \pm 2.3$  m\AA reported in the present work, the Li abundance would be 0.06 dex higher and the uncertainties larger at  $A_P(Li) = 2.09 \pm 0.08$  ( $1\sigma$ ). In this case the star moves further above the trend, but on account of its much larger error bars, has little impact on the slope.

clearly, as noted by those authors, more data are required at  $[\text{Fe}/\text{H}] < -3.5$  to place their result, and its implications for the primordial Li abundance, on a firmer basis.

We also note that to infer the primordial abundance from the observed one, a range of potentially systematic as well as random uncertainties needs to be taken into consideration. Furthermore, the computations of the primordial Li abundance as a function of baryon-to-photon ratio,  $\eta$ , or equivalently  $\Omega_B$ , are themselves subject to significant uncertainties. The impact of these issues is discussed more fully elsewhere (Ryan et al. 2000).

We are grateful to the Director and staff of the Anglo-Australian Observatory, and the Australian Time Allocation Committee for providing the observational facilities used in this study. We are likewise grateful to Dr D. Folha for obtaining the WHT spectrum as a Service Observation. It is a pleasure to thank Drs. R.D. Mathieu, P.E. Nissen, and J.A. Thorburn, for their generous assistance. J.E.N. gratefully acknowledges the support of the Department of Astronomy, University of Texas at Austin during the preparation of the manuscript, and T.C.B. acknowledges support of NSF grants AST 92-22326, AST 95-29454, and INT 94-17547. We also gratefully acknowledge the thorough report from Dr. P. Bonifacio, which led to a number of improvements to the text.

Table 1. EQUIVALENT WIDTHS FOR CS 22876-032A,B

$\lambda$ (Å) (1)	$\chi$ (eV) (2)	$\log gf$ (3)	$W_A$ (mÅ) (4)	$W_B$ (mÅ) (5)
Mg I				
3829.35	2.71	-0.48	57	29
5172.70	2.71	-0.38	51	24
5183.62	2.72	-0.16	59	29
Al I				
3944.01	0.00	-0.64	11	11
3961.52	0.00	-0.34	15	11
Si I				
3905.52	1.91	-1.09	15	17
Ca I				
4226.73	0.00	+0.24	34	18
Sc II				
4246.82	0.32	+0.32	<5	<5
Ti II				
3759.30	0.61	+0.20	28	14
3761.32	0.57	+0.10	21	9
Cr I				
4254.33	0.00	-0.11	<5	<5
Mn I				
4030.75	0.00	-0.62	<5	<5
Fe I				
3727.63	0.96	-0.62	24	12
3743.37	0.99	-0.78	27	<10
3758.24	0.96	-0.02	44	17
3763.80	0.99	-0.23	33	19
3787.88	1.01	-0.85	19	<10
3812.96	0.96	-1.03	13	13:
3815.84	1.48	+0.24	33	20
3820.43	0.86	+0.14	57	26
3825.88	0.92	-0.03	47	23
3827.82	1.56	+0.08	28	19
3849.97	1.01	-0.87	17	7
3856.37	0.05	-1.28	38	17

Table 1—Continued

$\lambda$ (Å) (1)	$\chi$ (eV) (2)	$\log gf$ (3)	$W_A$ (mÅ) (4)	$W_B$ (mÅ) (5)
3859.91	0.00	-0.70	62	22
3865.52	1.01	-0.97	14	12:
3872.50	0.99	-0.91	19	15
3878.02	0.96	-0.91	14	<7
3878.57	0.09	-1.36	33	18
3899.71	0.09	-1.52	28	18
3920.26	0.12	-1.74	21	15
3922.91	0.05	-1.64	24	15
3927.92	0.11	-1.52	24	16
3930.30	0.09	-1.49	28	17
4005.24	1.56	-0.60	12	10:
4045.81	1.48	+0.28	41	21
4063.59	1.56	+0.06	30	17
4071.74	1.61	-0.02	24	16
4132.06	1.61	-0.68	10	<5
4143.87	1.56	-0.20	13	9:
4202.03	1.48	-0.70	10	9:
4250.79	1.56	-0.71	8	<5
4260.47	2.40	+0.11	8	<5
4271.76	2.45	-0.34	28	12
4307.90	1.56	-0.07	25	15
4325.76	1.61	+0.01	25	16
4383.54	1.48	+0.20	37	16
4404.75	1.56	-0.13	23	15
4415.12	1.61	-0.62	11	7:
Co I				
3873.11	0.43	-0.66	<7	<7
Ni I				
3858.29	0.42	-0.95	<7	<7
Sr II				
4077.71	0.00	+0.15	<5	<5
Ba II				
4554.03	0.00	+0.16	<5	<5

Table 2. RADIAL VELOCITIES FOR CS 22876-032A,B

Date (1)	JD (2)	$V_A$ (3)	$\Delta V_A$ (4)	$V_B$ (5)	$\Delta V_B$ (6)	Source (7)
1985 Sep 6	2446315.1	-83.9	2.0	...	...	AAT, RGO <sup>a</sup>
1985 Dec 16	2446416.0	-96.8	2.0	...	...	AAT, RGO <sup>a</sup>
1989 Sep 13	2447783.2	-107.8	1.0	-74.8	1.0	AAT, UCLES <sup>b</sup>
1989 Oct 16	2447815.7	-103.1	1.0	-81.2	1.0	P.E. Nissen <sup>c</sup>
1989 Dec 6	2447867.0	-93.3	1.0	...	...	AAT, UCLES <sup>b</sup>
1990 Sep 27	2448162.1	-109.6	1.0	-76.2	1.0	AAT, UCLES <sup>b</sup>
1991 Aug 22	2448490.5	-87.0	2.0	...	...	AAT, UCLES <sup>b</sup>
1992 Aug 17	2448851.8	-78.6	1.0	-107.6	1.0	J.A. Thorburn <sup>d</sup>
1996 Aug 7	2450303.1	-110.2	1.0	-76.2	1.0	AAT, UCLES <sup>b</sup>
1997 Aug 23	2450683.8	-104.2	1.0	-81.3	1.0	AAT, UCLES <sup>b</sup>
1998 Aug 12	2451038.3	-87.8	1.0	-101.1	1.0	AAT, UCLES <sup>b</sup>
1999 Jul 29	2451388.7	-77.0	2.0	...	...	WHT, UES <sup>e</sup>
1999 Sep 23	2451444.6	-84.3	1.0	-105.5	1.0	AAT, UCLES <sup>b</sup>

<sup>a</sup>AAT, RGO spectrograph combination<sup>b</sup>AAT, University College London coudé échelle spectrograph combination<sup>c</sup>Private communication from P.E. Nissen. See Nissen (1989)<sup>d</sup>Private communication from J.A. Thorburn. See Thorburn & Beers (1993)<sup>e</sup>WHT, Utrecht échelle spectrograph combination; this closely matches the AAT, UCLES setup

Table 3. ORBITAL ELEMENTS OF CS 22876–032

Parameter (1)	Value (2)	s.e (3)	$\Delta^a$ (4)
Orbital period (days)	424.71	0.60	+0.18
$T_0$ (JD–2400000)	48576.37	13.51	+2.67
Eccentricity	0.12	0.03	–0.01
$\omega$ (degrees)	144.96	12.40	+2.95
Center-of-mass radial velocity (km s <sup>–1</sup> )	–93.36	0.28	–0.02
Primary:			
Radial vel. semi-amplitude ( $K_P$ ) (km s <sup>–1</sup> )	15.13	0.51	+0.03
Projected semi-major axis ( $a_P \sin(i)$ ) (km)	$8.77 \cdot 10^7$	$3.00 \cdot 10^6$	$0.03 \cdot 10^7$
$M_P \sin^3(i)$ ( $M_\odot$ )	0.76	0.04	0.01
Secondary:			
Radial vel. semi-amplitude ( $K_S$ ) (km s <sup>–1</sup> )	17.06	0.56	0.08
Projected semi-major axis ( $a_S \sin(i)$ ) (km)	$9.89 \cdot 10^7$	$3.25 \cdot 10^6$	$0.06 \cdot 10^7$
$M_S \sin^3(i)$ $M_\odot$	0.68	0.04	0.01
$M_S/M_P$	0.89	0.04	0.00

<sup>a</sup>Element change when two most discrepant points are removed from the sample.

Table 4. PHYSICAL PARAMETERS FOR CS 22876–032

Color <sub>A+B</sub> (1)	M <sub>P</sub> (2)	T <sub>P</sub> (3)	Color <sub>P</sub> (4)	f <sub>4300,P</sub> <sup>a</sup> (5)	M <sub>S</sub> (6)	T <sub>S</sub> (7)	Color <sub>S</sub> (8)	f <sub>4300,S</sub> <sup>a</sup> (9)	[Fe/H] (10)	M <sub>S</sub> /M <sub>P</sub> (11)
Individual:										
<i>B</i> – <i>V</i> = 0.395	0.841	6425	0.360	1.28	0.743	5700	0.515	4.6	–3.60	0.883
<i>V</i> – <i>R</i> = 0.280	0.825	6250	0.258	1.29	0.723	5575	0.345	4.5	–3.75	0.876
<i>R</i> – <i>I</i> = 0.310	0.819	6225	0.287	1.26	0.711	5500	0.375	4.9	–3.78	0.868
Mean:										
	0.828	6300		1.28	0.726	5592		4.7	–3.71	0.876

<sup>a</sup>Equivalent width correction factor at  $\lambda$ 4300 Å.

Table 5. ADOPTED ATMOSPHERIC PARAMETERS FOR CS 22876–032

Component (1)	$T_{\text{eff}}$ (2)	$\log g$ (3)	[Fe/H] (4)	$\xi^a$ (5)	$f_{4300}$ (6)
Primary	6300	4.5	–3.71	1.4	1.28
Secondary	5600	4.5	–3.71	1.0	4.60

<sup>a</sup>Microturbulent velocity (km s<sup>–1</sup>)

Table 6. ERROR BUDGET FOR CS 22876-032

Error Source (1)	$\Delta$ (2)	$\Delta[\text{Fe}/\text{H}]_{\text{P}}$ or $\Delta(M_{\text{S}}/M_{\text{P}})$ (3)
Impact on Systemic [Fe/H]:		
Atmospheric parameters:		
$T_{\text{eff},\text{P}}$	130 K	0.10
$T_{\text{eff},\text{S}}$	130 K	0.03
Microturbulence, $\xi_{\text{P}}$	0.3 km s <sup>-1</sup>	0.03
Surface Gravity, $\log g_{\text{P}}$	0.3 dex	0.01
Model Atmosphere Grid		
Temperature gradient	...	0.10
Isochrones:		
Metallicity, $\log Z$	0.50 dex	0.04
Adopted Age	2 Gyr	0.04
Adopted Helium, Y	0.05	0.00
Impact on Mass Ratio ( $M_{\text{S}}/M_{\text{P}}$ ):		
Atmospheric parameters:	as above	0.02
Isochrones:	as above	0.03

Table 7. SOURCES OF [Fe/H] DIFFERENCES

Source (1)	NPB <sup>a</sup> (2)	This work (3)	[Fe/H] <sub>This</sub> –[Fe/H] <sub>NPB</sub> (4)
$T_{\text{eff}}$ (K)	6000	6300	+0.24
$\log g$ (cgs)	4.0	4.5	<0.02
$\xi$ (km s <sup>-1</sup> )	2.0	1.4	+0.05
$W_{\lambda}$	As observed	Corrected <sup>b</sup>	-0.03
$\log gf$	Laboratory	Laboratory	< 0.02
Models	Kurucz (1993)	Bell (1983)	-0.12
Model [Fe/H]	-4.0	-2.0	+0.04
$\log (N_{\text{Fe}}/N_{\text{H}})_{\odot}$	-4.33	-4.50	+0.17

<sup>a</sup>Norris et al.(1993)

<sup>b</sup>Present measures are 0.08 dex smaller than those of NPB, but were multiplied by  $f_{4300,\text{P}} = 1.28$ .

Table 8. RELATIVE ABUNDANCES, [X/Fe], FOR CS 22876–032

Element (1)	Feature (2)	log (N/N <sub>H</sub> ) <sub>○</sub> (3)	[X/Fe] <sub>P</sub> (4)	s.e (5)	[X/Fe] <sub>S</sub> (6)	s.e (7)
Mg	3	−4.42	0.50	0.12	0.51	0.15
Al <sup>a</sup>	3961 Å	−5.53	−0.45	0.12	−0.42	0.23
Si	3905 Å	−4.45	−0.21	0.13	0.29	0.24
Ca	4226 Å	−5.64	+0.01 <sup>b</sup>	0.13	−0.01 <sup>b</sup>	0.24
Sc	4246 Å	−8.90	< 0.27	0.07	...	...
Ti	2	−7.01	0.08	0.11	0.23	0.23
Cr	4254 Å	−6.33	<−0.22	0.04	...	...
Mn	4030 Å	−6.61	<−0.18	0.04	<−0.26	0.06
Co	3873 Å	−7.08	< 1.25	0.04	...	...
Ni	3858 Å	−5.75	< 0.00	0.04	...	...
Sr	4077 Å	−9.10	<−0.65	0.05	...	...
Ba	4554 Å	−9.87	< 0.38	0.07	...	...

<sup>a</sup>From Al 3944 Å, [Al/Fe]<sub>P</sub> = −0.32 and [Al/Fe]<sub>S</sub> = −0.13, respectively. As emphasized first by Arpigny & Magain (1983) this line suffers from potential blending with a feature of CH, and is accordingly excluded from many analyses (e.g. Ryan et al. 1996), including the present work. For CS 22876–032 this may explain the higher abundance derived from the  $\lambda$  3944 Å line in the secondary.

<sup>b</sup>Following Magain (1988) and Ryan et al. (1991, 1996) we have applied a correction of +0.18 dex to the abundances determined from Ca I 4226 Å. This line consistently yields a lower abundance than other Ca I lines.

## REFERENCES

Arpigny, C. & Magain, P. 1983, A&A, 127, L7

Baumüller, D. & Gehren, T. 1997, A&A, 325, 1088

Beers, T.C., Preston, G.W., & Shectman, S.A. 1985, AJ, 90, 2089

Beers, T.C., Preston, G.W., & Shectman, S.A. 1992, AJ, 103, 1987

Beers, T.C., Rossi, S., Norris, J.E., Ryan, S.G., Molaro, P., & Rebolo, R. 1998, Sp.Sci.Rev. 84, 139

Bell, R.A. 1983, private communication

Binnendijk, L. 1960, Properties of Double Stars; A Survey of Parallaxes and Orbits, (Philadelphia: Univ. of Pennsylvania Press), 163

Bergbusch, P.A. & VandenBerg, D.A. 1992, ApJS, 81, 163

Bessell, M.S. & Norris, J. 1984, ApJ, 285, 622

Cowan, J.J., Pfeiffer, B., Kratz, K.-L., Thielemann, F.-K., Sneden, C., Burles, S., Tytler, D., & Beers, T.C. 1999, ApJ, 521, 194

Green, E.M., Demarque, P., & King, C.R. 1987, *The Revised Yale Isochrones and Luminosity Functions* (New Haven: Yale University Observatory)

Ikuta, C. & Aromoto, N. 1999, PASJ, 51, 459

Keeping, E.S. 1962, Introduction to Statistical Inference (Princeton: Van Nostrand), 202

Kurucz, R.L. 1993, CD-ROM 13, ATLAS9 Stellar Atmospheres Program and 2 km/s Grid (Cambridge : Smithsonian Astrophys. Obs.)

Lafler, J. & Kinman, T.D. 1965, ApJS, 11, 216

Lehmann-Filhés, R. 1894, Astron. Nach., 136, 17

Magain, P. 1988, in IAU Symp. 132, The Impact of Very High S/N Spectroscopy on Stellar Physics, ed. G. Cayrel de Strobel & M. Spite (Dordrecht: Kluwer), 485

McWilliam, A., Preston, G.W., Sneden, C., & Searle, L. 1995, AJ, 109, 2757

Molaro, P. & Castelli, F. 1990, A&A, 228, 426

Nakamura, T., Umeda, H., Nomoto, K., Thielemann, F.-K., & Burrows, A. 1999, ApJ, 517, 193

Nissen, P.E. 1989, The Messenger, 58, 40

Norris, J.E. 1999, The Third Stromlo Symposium: The Galactic Halo, eds. B.K.Gibson, T.S. Axelrod, and M.E.Putman (San Francisco: ASP), 213

Norris, J.E., Peterson, R.C., & Beers, T.C. 1993, ApJ, 415, 797

Norris, J.E., Ryan, S.G., & Beers, T.C. 1996, ApJS, 107, 391

Peterson, R.C. & Carney, B.W. 1989, ApJ, 347, 266

Primas, F., Molaro, P., & Castelli, F. 1994 A&A, 290, 885

Russell, H.N. 1902, ApJ, 15, 252

Ryan, S.G. 1998, A&A, 331, 1051

Ryan, S.G. 2000, in The Galactic Halo: From Globular Clusters to Field Stars eds. A. Noels and P. Magian (Liège: Université de Liège), in press

Ryan, S.G., Beers, T.C., Olive, K.A., Fields, B.D., & Norris, J.E., 2000, ApJ, 530, L57

Ryan, S.G., Norris, J.E., & Beers, T.C. 1996, ApJ, 471, 254

Ryan, S.G., Norris, J.E., & Beers, T.C. 1999, ApJ, 523, 654

Ryan, S.G., Norris, J.E., & Bessell, M.S. 1991, AJ, 102, 303

Schuster, W.J., Nissen, P.E., Parrao, L., Beers, T.C., & Overgaard, L.P. 1996, A&AS, 117, 317

Schuster, W.J., Parrao, L., & Contreras Martinez, M.E. 1993, A&AS, 97, 951

Shigeyama, T. & Tsujimoto, T. 1998, ApJ, 507, L135

Thorburn, J.A. 1994, ApJ, 421, 318

Thorburn, J.A. & Beers, T.C. 1993, ApJ, 404, L13

Tsujimoto, T. & Shigeyama, T. 1998, ApJ, 508, L151

Tsujimoto, T., Shigeyama, T., & Yoshii, Y. 1999, ApJ, 519, L63

Underhill, A.B. 1966, The Early Type Stars,(New York: Gordon & Breach), 127

Weaver, T.A. & Woosley, S.E. 1993, Phys. Rep., 227, 65

Wolfe, R.H., Horak, A.G., & Storer, N.W. 1967, in Modern Astrophysics; A Memorium to Otto Struve, ed. M. Hack (New York: Gordon & Breach), 251

Woosley, S.E. & Weaver, T.A. 1995, ApJS, 101, 181

VandenBerg, D.A. & Bell, R.A. 1985, ApJS, 58, 561

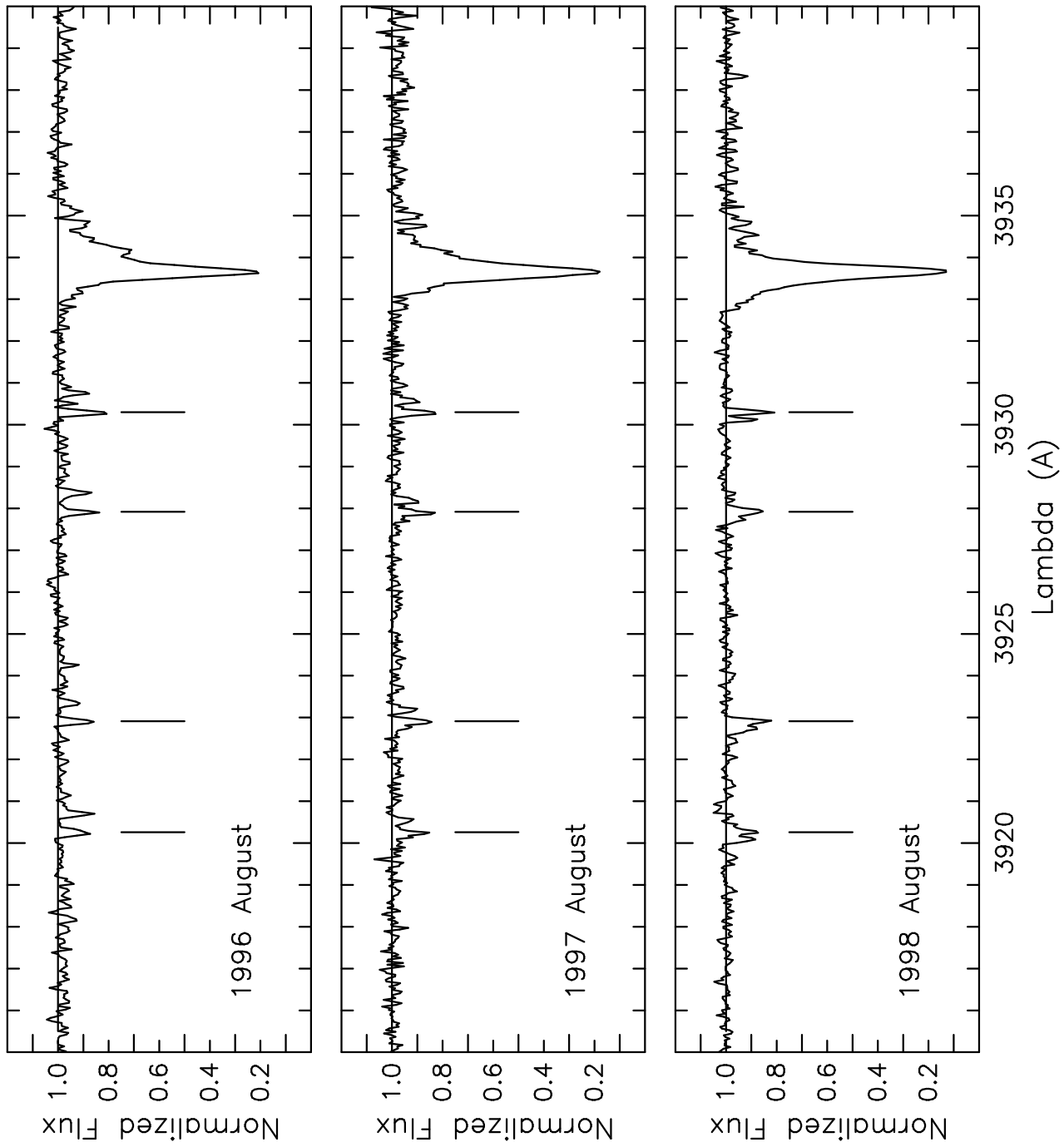


Fig. 1.— Spectra of CS 22876–032 in the region of the Ca II K line. The vertical lines indicate the positions of Fe I lines in the primary component.

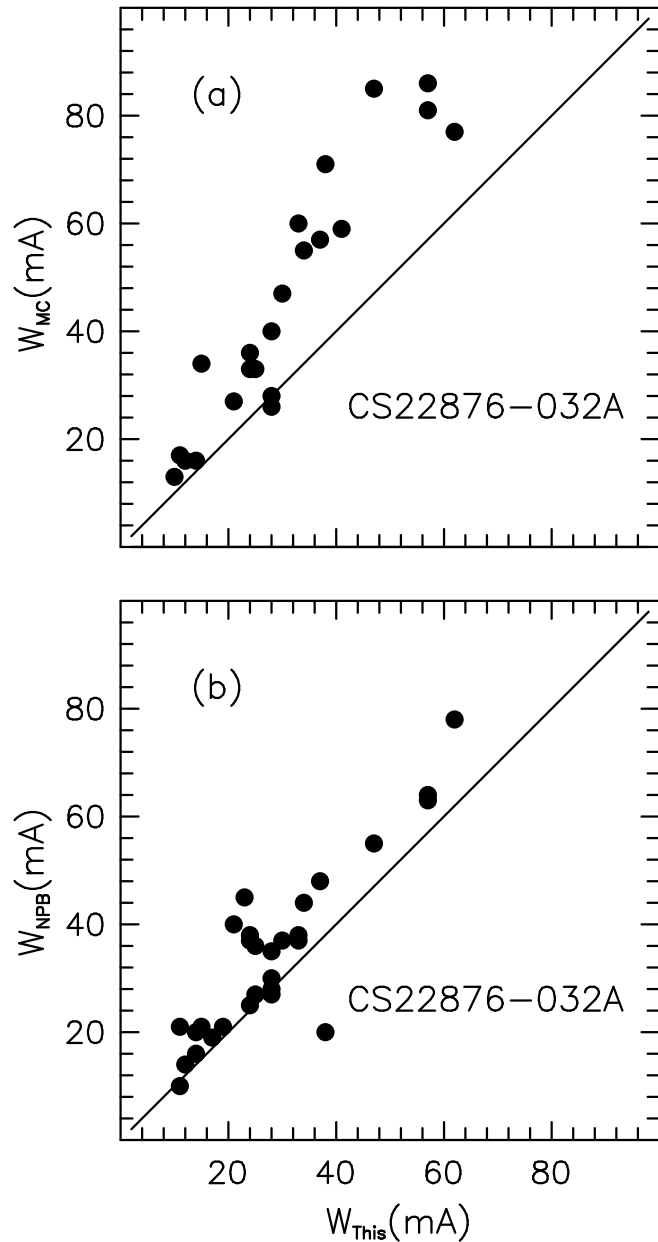


Fig. 2.— Comparison of the equivalent widths presented here for CS 22876–032A with those of (a) Molaro and Castelli (1990) and (b) Norris et al. (1993).

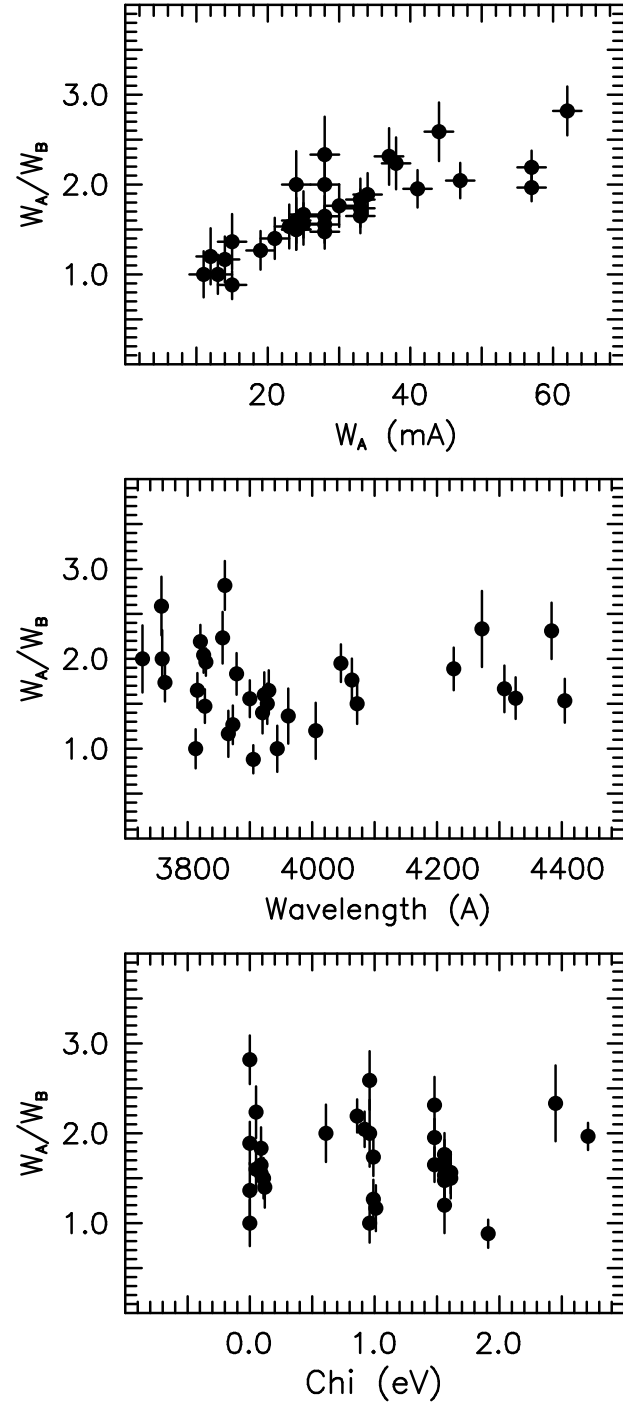


Fig. 3.— The dependence of  $W_A/W_B$  on  $W_A$ , wavelength, and excitation potential.

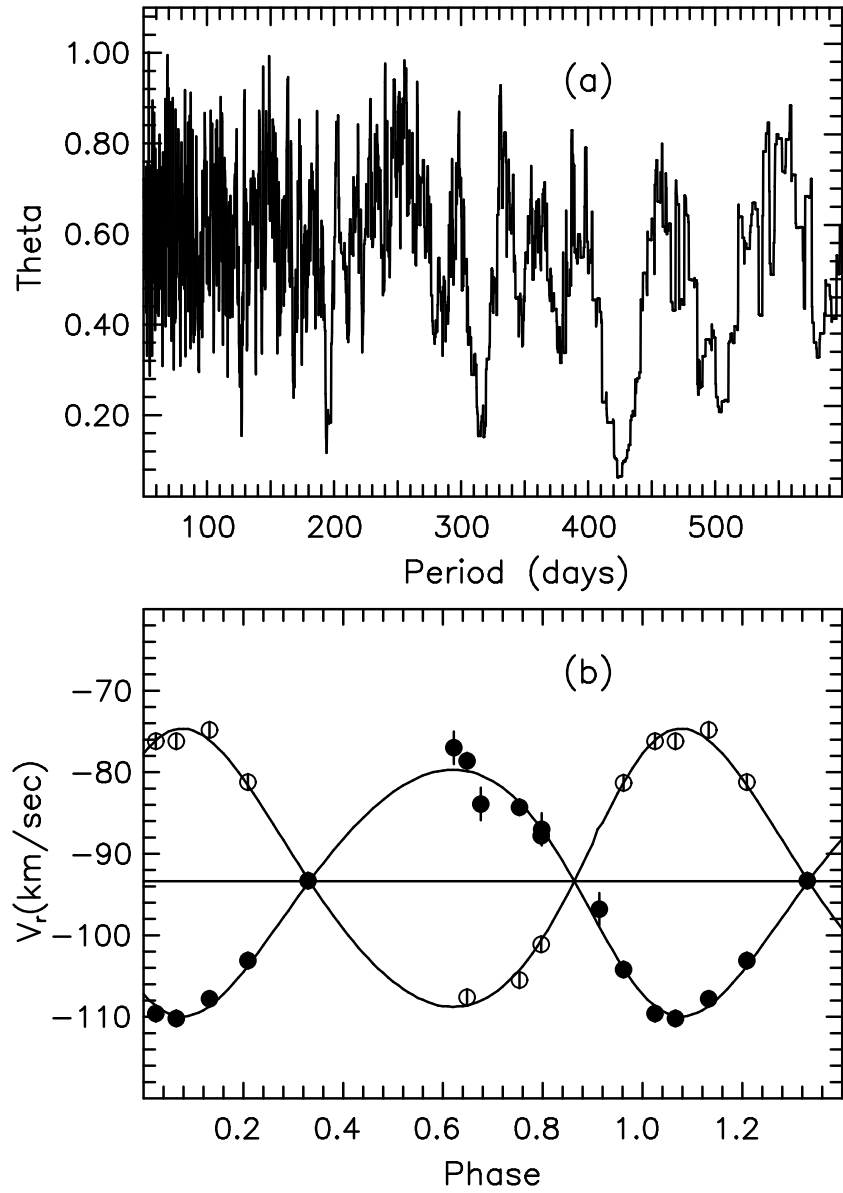


Fig. 4.— (a) Periodogram of radial velocities for CS 22876–032. ('Theta' is as defined by Lafler & Kinman (1965, Eqn. 1).) (b) Radial velocity curves for CS 22876–032A (filled symbols) and CS 22876–032B (open symbols) for period 424.71 days.  $1\sigma$  error bars, comparable in size to the symbols, are also shown. The curves are determined by the elements in Table 3, while the horizontal line represents the center-of-mass velocity of the system.

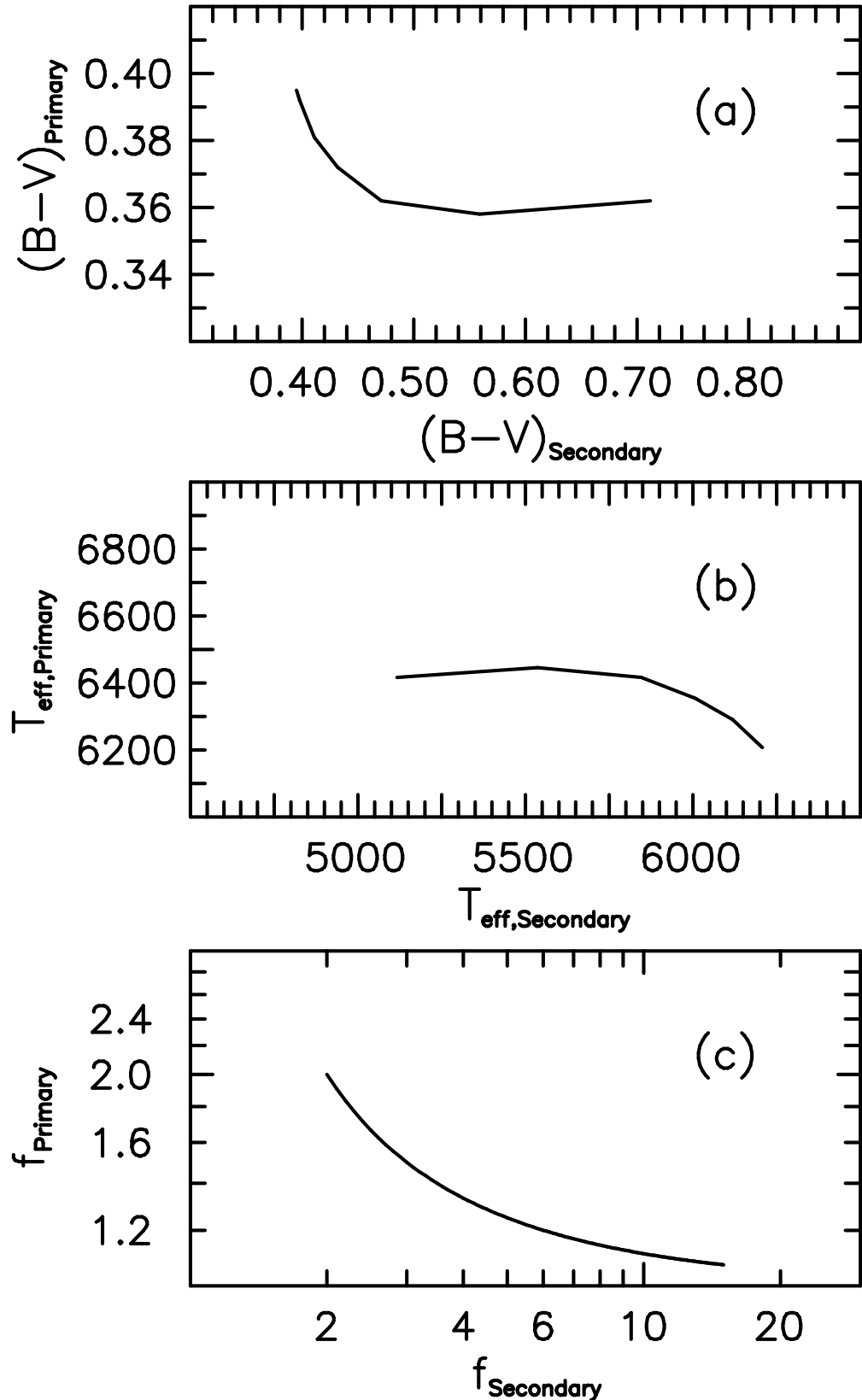


Fig. 5.— Locus of primary, secondary isochrone pairs of (a)  $B-V$ , (b)  $T_{\text{eff}}$ , and (c) equivalent width correction factors,  $f$  (applicable at  $\lambda 4300 \text{ \AA}$ ), consistent with  $B-V = 0.395$  observed

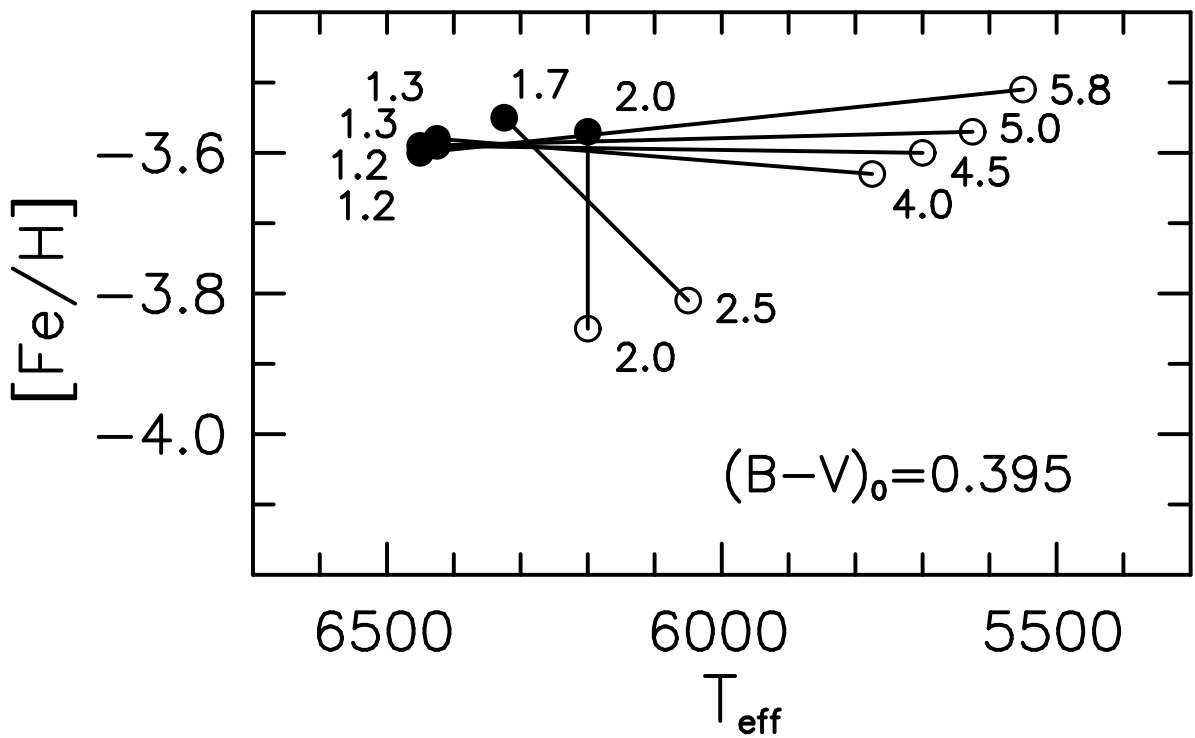


Fig. 6.— The dependence of  $[Fe/H]$  on  $T_{\text{eff}}$  for pairs of primary and secondary isochrone components defined by the observed  $B-V$  and model atmosphere analysis of the Fe I line strengths. Filled and open symbols refer to primary and secondary, respectively, and members of pairs are joined by lines. The equivalent width correction factors,  $f_{4300}$ , are appended to the data points. See text for discussion.

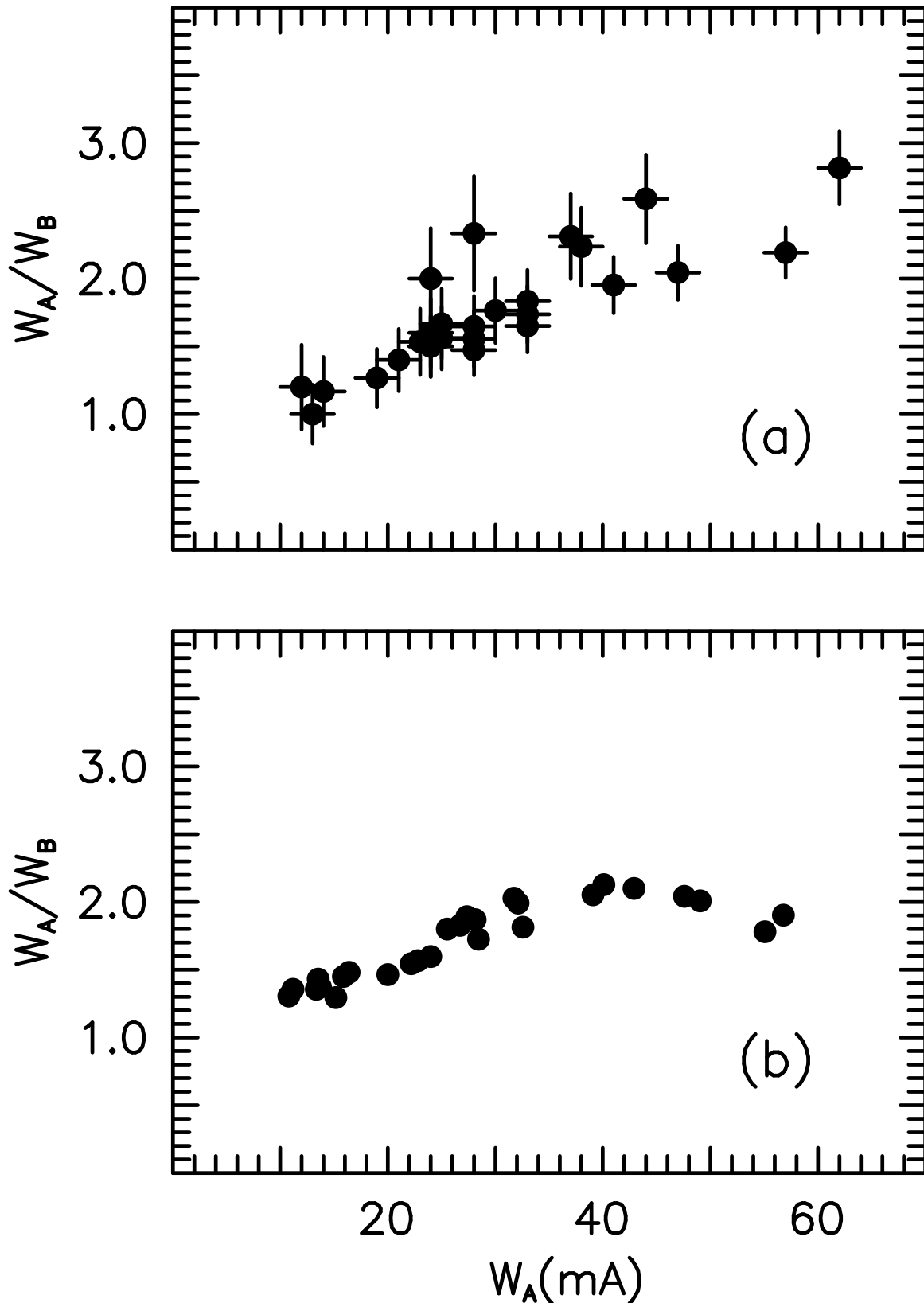


Fig. 7.— A comparison of (a) the observed and (b) predicted dependence of  $W_A/W_B$  on  $W_A$  for CS 22876-032. In both panels only Fe I lines stronger than 10 mÅ in both components

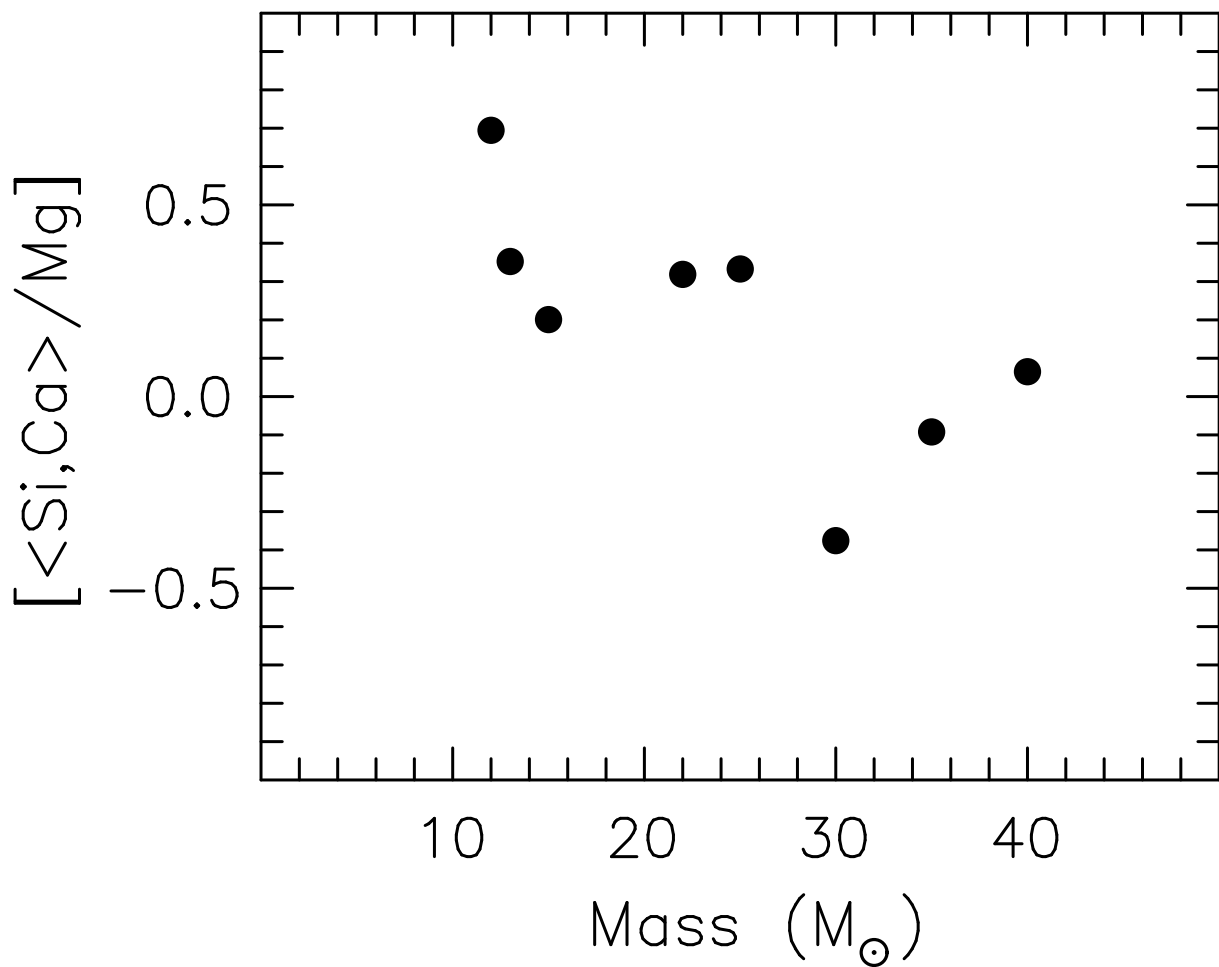


Fig. 8.— The dependence of  $[\langle \text{Si,Ca} \rangle / \text{Mg}]$  on supernova mass, from the models of Woosley & Weaver (1995). See text for discussion.

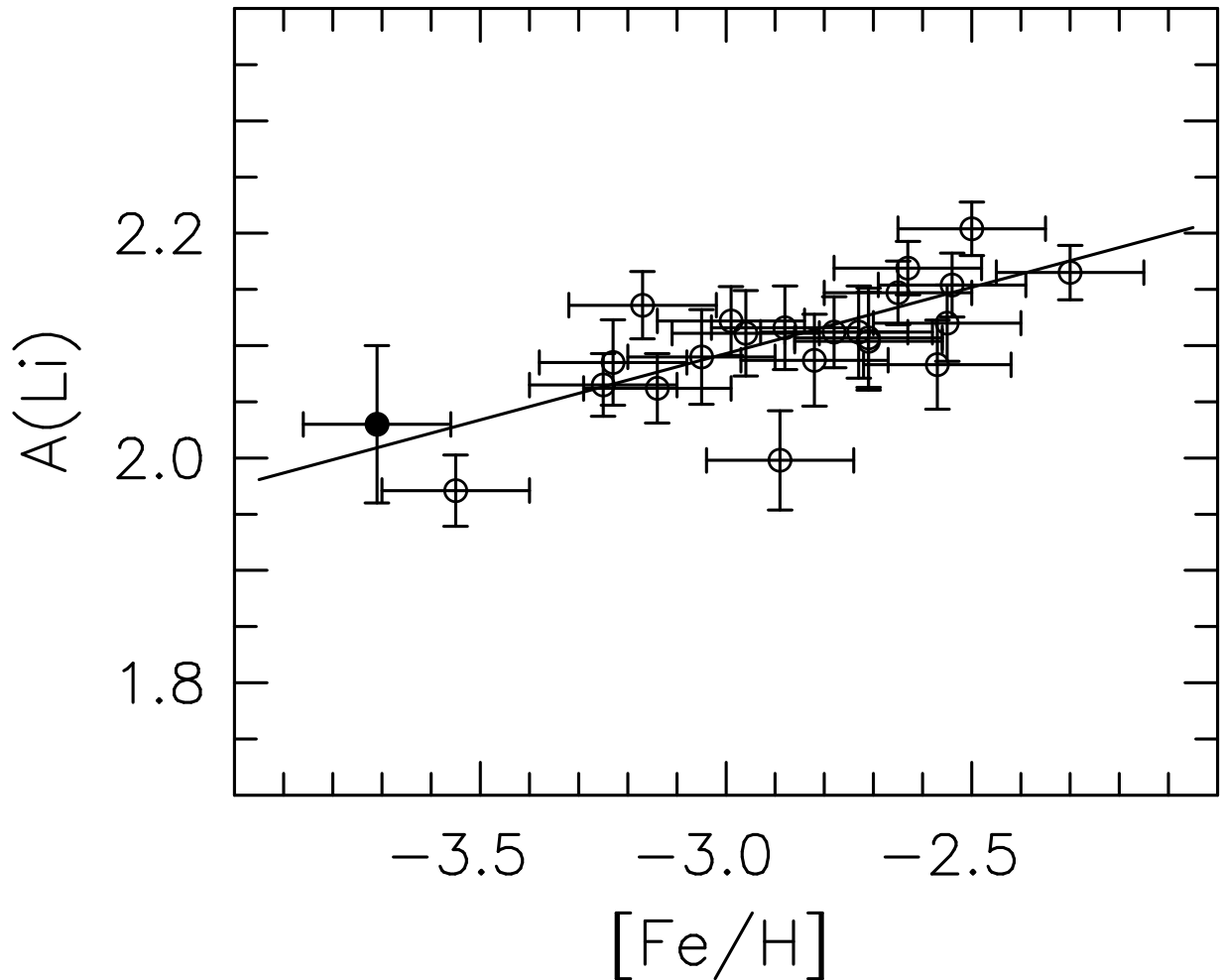


Fig. 9.— A comparison of the lithium abundance of CS 22876–032 (filled symbol) with those of the unbiased near-main-sequence-turnoff sample of Ryan et al. (1999) (open symbols). The regression line  $A(\text{Li}) = 2.447 + 0.118 \times [\text{Fe}/\text{H}]$  of Ryan et al. is also shown.